Supplementary Information for

The unexpectedly short Holocene Humid Period in Northern Arabia

Ina Neugebauer[1,2], Michèle Dinies[3,4], Birgit Plessen[1], Nadine Dräger[1], Achim Brauer[1], Helmut Brückner[5], Peter Frenzel[6], Gerd Gleixner[7], Philipp Hoelzmann[4], Kim Krahn[8], Anna Pint[6], Valérie F. Schwab[7], Anja Schwarz[8], Rik Tjallingii[1] and Max Engel[9,10,*]

1 GFZ German Research Centre for Geosciences, Section Climate Dynamics and Landscape Evolution, Telegrafenberg, 14473 Potsdam, Germany
2 University of Geneva, Department of Earth Sciences, Rue des Maraichers 13, 1205 Genève, Switzerland
3 German Archaeological Institute (DAI), Scientific Department of the Head Office, Im Dol 2-6, 14195 Berlin, Germany
4 Freie Universität Berlin, Institute of Geographical Sciences, Malteser Str. 74-100, 12249 Berlin, Germany
5 University of Cologne, Institute of Geography, Zülpicher Str. 45, 50674 Köln, Germany
6 Friedrich Schiller University Jena, Institute of Earth Sciences, Burgweg 11, 07749 Jena, Germany
7 Max Planck Institute for Biogeochemistry, Research Group Molecular Biogeochemistry, Hans-Knöll-Str. 10, 07745 Jena, Germany
8 Technische Universität Braunschweig, Institute of Geosystems and Bioindication, Langer Kamp 19c, 38106 Braunschweig, Germany
9 Heidelberg University, Institute of Geography, Im Neuenheimer Feld 348, 69120 Heidelberg, Germany
10 Royal Belgian Institute of Natural Sciences, Geological Survey of Belgium, Jennerstraat 13, 1000 Brussels, Belgium
* Corresponding author: Max Engel, max.engel@uni-heidelberg.de

Regional setting of Tayma

The sabkha N of the town of Tayma fills a closed basin overlying Lower Ordovician micaceous siltstones (Qasim Formation), with an extension of approximately 20 km^2 and a hydrological catchment 660 km^2[1,2] (Supplementary Fig. 1). Today, the deepest point of the sabkha is at about 800 m a.s.l. The depression has developed in a NW–SE trending graben structure above the Ordovician Qasim Formation (Supplementary Fig. 1c). The northern rim consists of a staircase of steep, slightly northwards dipping sandstones and micaceous siltstones of this formation with a maximum height at about 860 m a.s.l. (Supplementary Fig. 1a). To the S, the surface gradually rises towards the town situated above the basin at about 830 m a.s.l., from where the underlying Ordovician Saq sandstone continuously rises up to 1000 m a.s.l. These about 600 m-thick medium to coarse-grained sandstones form the main groundwater-bearing layer of the W Peninsula, the Saq aquifer[3] (Supplementary Fig. 1c). The groundwater flow coming from the SE[4] is under artesian pressure due to the graben structure of the Tayma basin. Potential surface waters drain by several small inflows and wadis into the endorheic basin (Supplementary Fig. 1b).

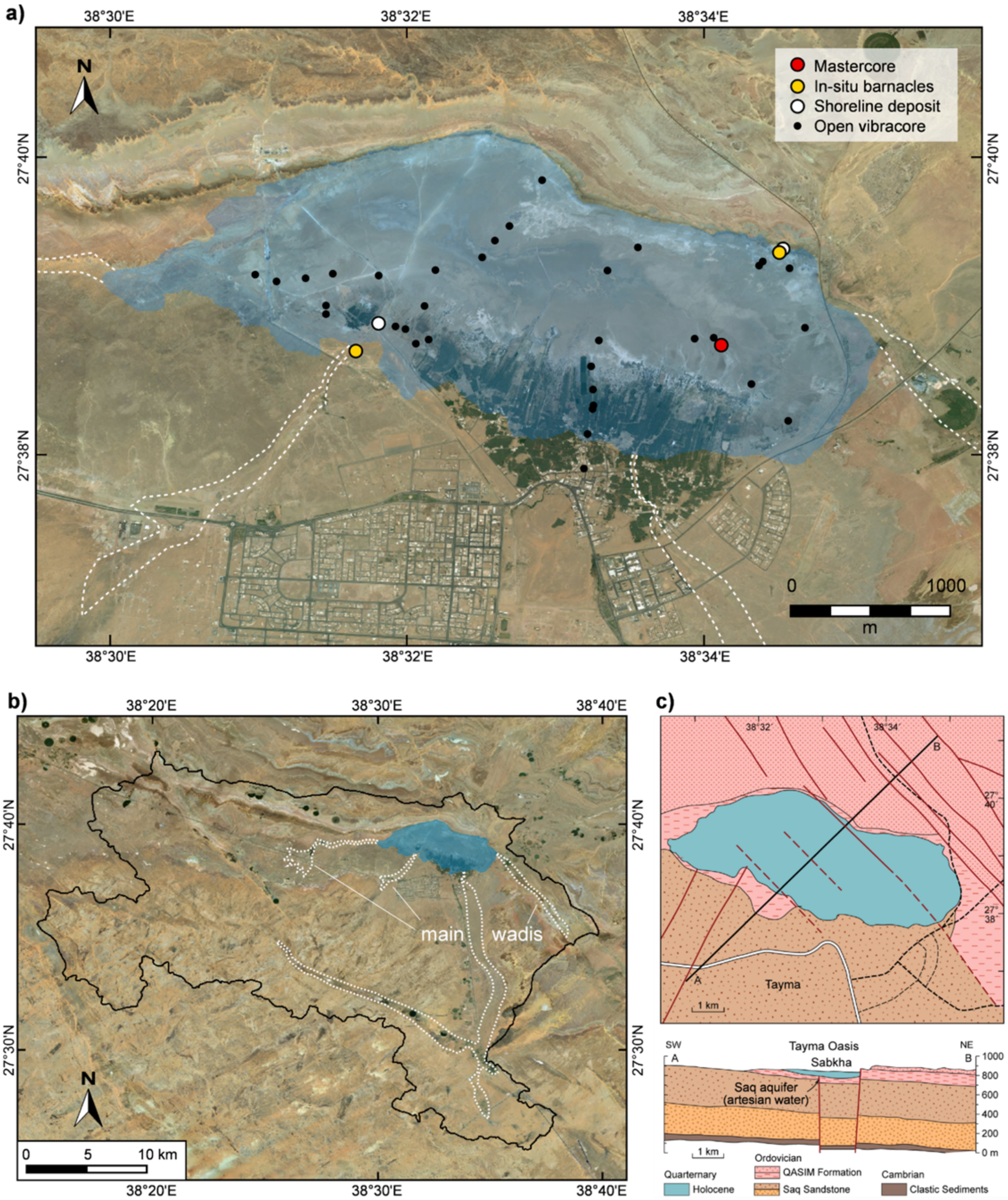

Supplementary Fig. 1: Local setting of the Tayma palaeolake. (a) Tayma palaeolake as reconstructed from highest shoreline deposits[1], a digital elevation model based on local DGNSS and global SRTM data[2] and a large dataset of vibracores (basemap: Landsat/Copernicus, accessed through Google Earth Pro). The main wadis entering the endorheic basin are marked by white dashed lines. (b) Surface catchment of the Tayma palaeolake[5] showing the spatial extent of the main wadis (basemap: Landsat/Copernicus, accessed through Google Earth Pro). (c) Simplified geology and tectonic features of the oasis of Tayma creating the artesian groundwater source, shown as top view and stratigraphic profile based on ref.[6].

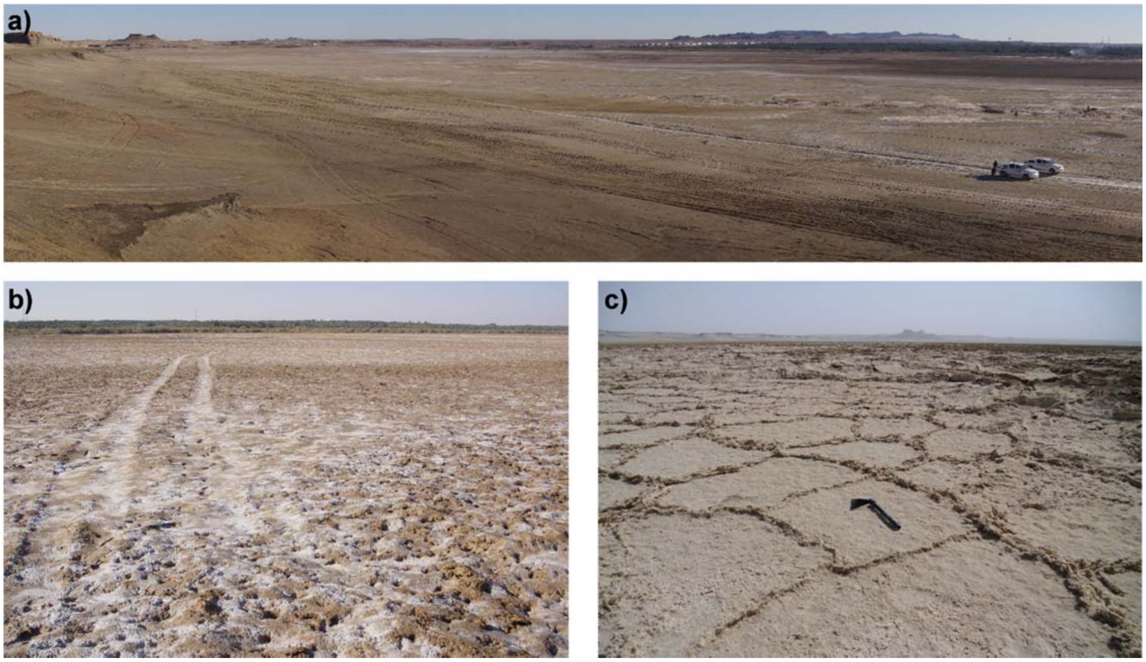

Supplementary Fig. 2: Views of the sabkha of Tayma. (a) Panoramic view from the NW margin on top of the lowermost escarpment towards SE, overlooking the sabkha. Zeugenbergs in the upper left represent remnants of higher escarpment levels. The upper right shows the palm gardens bordering the sabkha in the S as well as some buildings of the easternmost part of the oasis of Tayma. (b) Typical gypsum buckled-crust surface of the central part of the sabkha, thinly covered by Na salts. (c) In some more central parts, the buckled crust gives way to massive salt polygons.

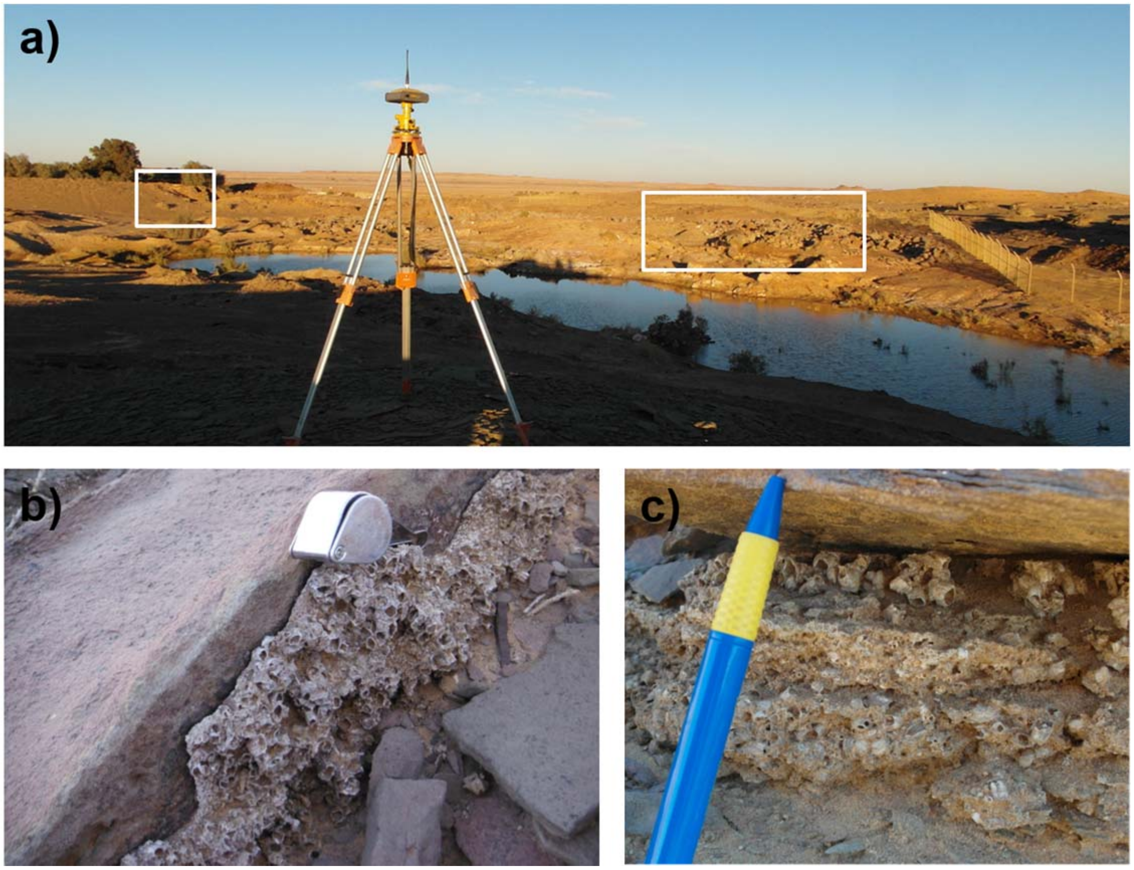

Supplementary Fig. 3: SW barnacle colonies. (a) Overview of the SW major wadi entering the sabkha basin (Supplementary Fig. 1a). (b), (c) Along both wadi margins, *in-situ* Holocene barnacle colonies are preserved at elevations of c. 12 m above the present sabkha floor, representing palaeo-shoreline indicators of the peak phase of the early to mid-Holocene lake (SW yellow dot in Supplementary Fig. 1a).

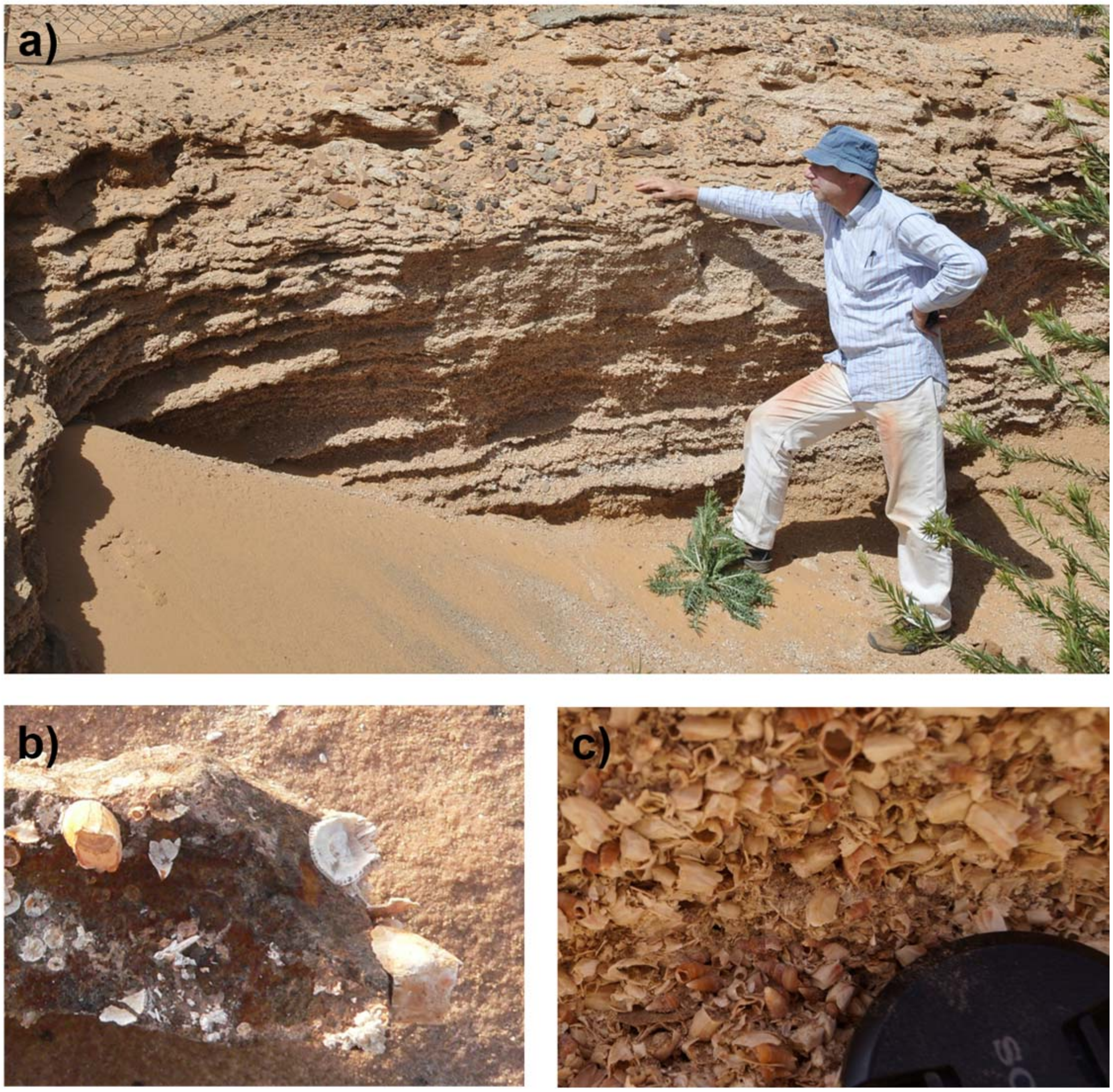

Supplementary Fig. 4: SW bioclastic deposit. (a) Stratified lake-shoreline deposit almost entirely consisting of barnacles, gastropod, ostracod and foraminifer shells and tests, as well as quartz sand (thickness ca. 2.3 m; SW white dot in Supplementary Fig. 1a). Shells were dated to the early Holocene (profile TAY 180 in refs.[1,7]). (b) *In-situ* barnacles attached to local Ordovician siltstone clasts floating in the bioclastic matrix. (c) Close-up of the texture in (a).

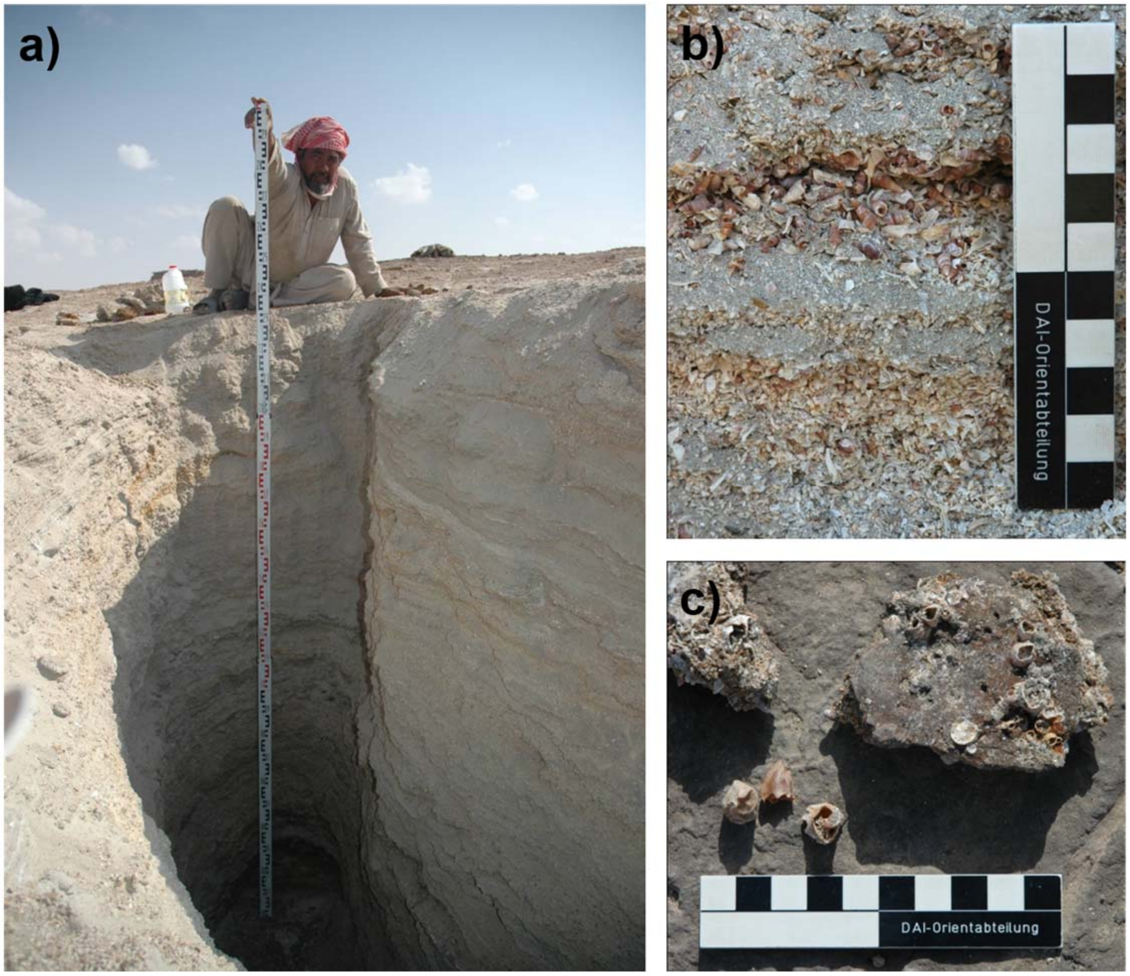

Supplementary Fig. 5: NE bioclastic deposit. (a) Stratified lake-shoreline deposit almost entirely consisting of barnacles, gastropod, ostracod and foraminifer shells and tests, as well as quartz sand (NE yellow and white dots in Supplementary Fig. 1a). Shells were dated to the early Holocene (profile TAY 177 in ref.[1]). (b) Close-up of the texture in (a). (c) *In-situ* Holocene barnacles attached to local Ordovician siltstone at the base of the profile.

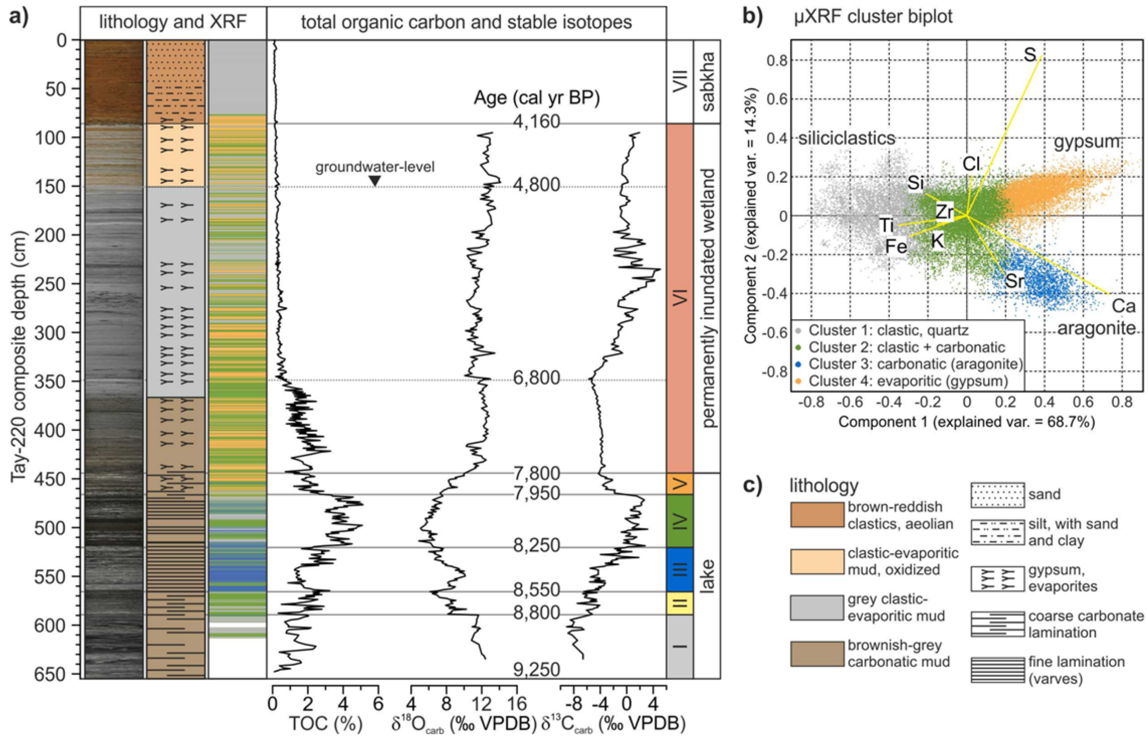

Supplementary Fig. 6: Lithology and sediment geochemistry of the Tayma composite profile. (a) Core scans, lithological description, down-core clustering results from XRF elemental scanning data (see (b) for legend), total organic carbon content (TOC)[8], $\delta^{18}O_{carb}$ and $\delta^{13}C_{carb}$ stable isotopes data, and discrimination of lake phases; the recent (in 2015) groundwater level at 1.5 m depth is marked with black triangles. (b) Principal-component biplot of XRF core-scanning results showing the statistical clusters; principal components 1+2 explain 83% of the variance. (c) Legend for the lithological description.

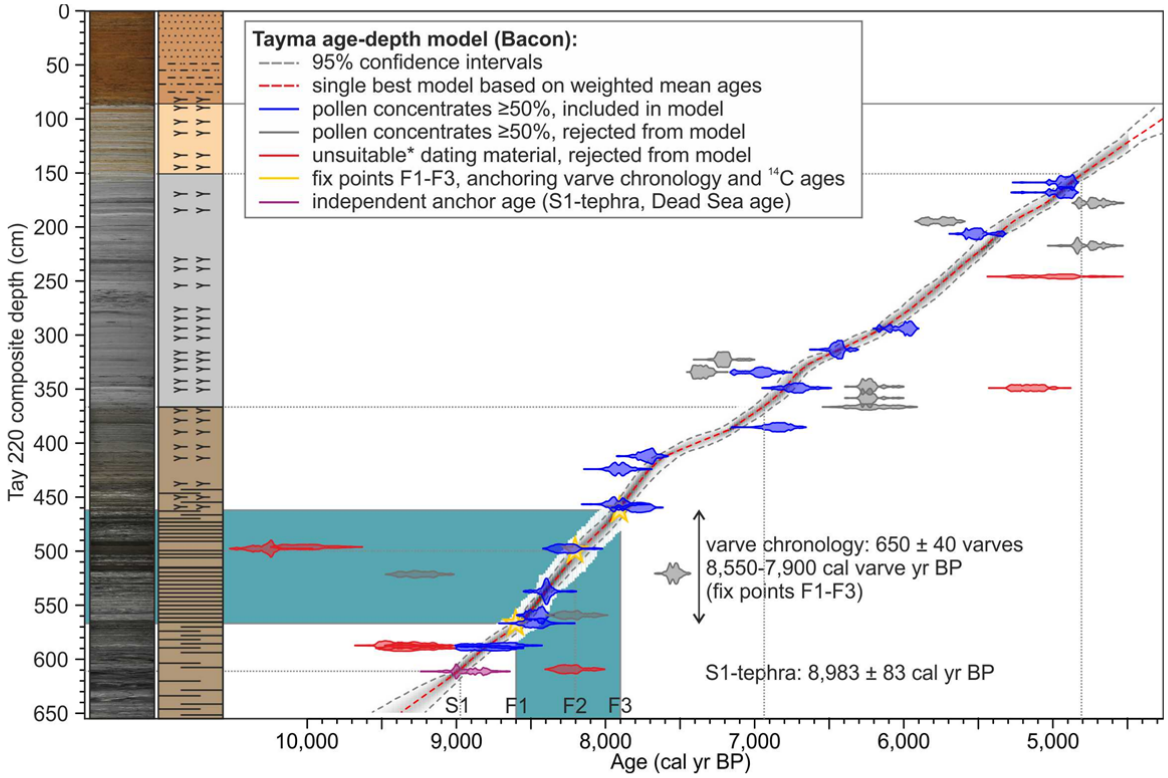

Supplementary Fig. 7: Age-depth model of the Tayma sediment composite profile. The age-depth model was constructed with Bacon v2.2 using flexible Bayesian modelling[9] including implemented outlier analysis and the IntCal13 atmospheric calibration curve[10] (see Methods). The model is based on radiocarbon ages of pollen concentrates, an independent anchor age of the S1-tephra[11] and a varve chronology between 8,550 and 7,900 cal varve yr BP (Tayma deep-lake phases III and IV; marked with a blue rectangle).

Supplementary Table 1: AMS-radiocarbon dating results from Tayma sediment cores. Bold font: sample age included in Bayesian age model (Bacon with implemented outlier analysis); normal font: sample material is suitable (pollen concentration ≥50%), but age is rejected from the Bacon age model; italic font: sample material is not suitable (pollen concentration <50%, dated material is affected by hard-water effect, or amount of datable carbon is too low) and age is rejected from the Bacon age model; na – information not available.

Sample ID	Core	Core segment	Segment depth (cm)	Tay 220 composite depth (cm)	Lab no.	^{14}C age BP (± 1σ)	C (mg)	Dated material	Calibrated age range (95.4%)	Calibrated median age BP (± 1σ)
AMS_20	**Tay 254**	**1-2**	**65-74.5**	**159**	**Poz-62344**	**4,345 ± 35**	**0.5**	**75% pollen**	**4,845-5,033**	**4,914 ± 47**
AMS_21	**Tay 254**	**1.5-2.5**	**3-12**	**168.25**	**Poz-62562**	**4,360 ± 40**	**na**	**80% pollen**	**4,849-5,039**	**4,927 ± 61**
AMS_22	Tay 254	1.5-2.5	12-22	178	Poz-62345	4,200 ± 40	0.5	85% pollen	4,588-4,849	4,730 ± 69
AMS_3	Tay 220	2-3	11-18	195	Poz-55862	5,010 ± 50	0.4	60% pollen	5,645-5,900	5,750 ± 77
AMS_23	**Tay 254**	**1.5-2.5**	**43-53**	**206.5**	**Poz-62553**	**4,780 ± 50**	**0.5**	**80% pollen**	**5,327-5,604**	**5,514 ± 71**
AMS_2	Tay 220	1.5-2.5	88-93	217.5	UGAMS-12598	4,240 ± 45	na	50% pollen	4,619-4,873	4,798 ± 75
AMS_4	*Tay 220*	*2-3*	*64-68*	*246*	*Poz-55866*	*4,360 ± 100*	*0.1*	*plant fibre fragment*	*4,651-5,306*	*4,976 ± 158*
AMS_30	**Tay 254**	**2-3**	**67-77**	**294**	**Poz-62556**	**5,240 ± 35**	**na**	**70% pollen**	**5,918-6,177**	**5,986 ± 70**
AMS_31	**Tay 254**	**2.5-3.5**	**9-18**	**313.5**	**Poz-62347**	**5,660 ± 30**	**na**	**70% pollen**	**6,324-6,503**	**6,440 ± 35**
AMS_43	Tay 254	2.5-3.5	19-25	322.75	Poz-79480	6,275± 35	0.6	60% pollen	7,030-7,275	7,212 ± 42
AMS_53	**Tay 220**	**2.5-3.5**	**58-63**	**334.5**	**Poz-87384**	**6,090 ± 40**	**0.5**	**70% pollen**	**6,803-7,156**	**6,957 ± 77**
AMS_44	Tay 254	2.5-3.5	29-36	335	Poz-79481	6,420± 35	0.8	85% pollen	7,278-7,422	7,357 ± 42
AMS_32	Tay 254	2.5-3.5	43-49	347.75	Poz-62557	5,430 ± 40	0.6	95% pollen	6,126-6,303	6,238 ± 45
AMS_1a	**Tay 220**	**3-4**	**2-5**	**349**	**UGAMS-12596**	**5,900 ± 55**	**na**	**55% pollen**	**6,567-6,883**	**6,723 ± 68**
AMS_1b	*Tay 220*	*3-4*	*2-5*	*349*	*UGAMS-12597*	*4,500 ± 40*	*na*	*70% charred plant particles*	*4,982-5,305*	*5,163 ± 84*
AMS_33	Tay 254	2.5-3.5	49-63	357.75	Poz-62559	5,435 ± 35	na	80% pollen	6,187-6,296	6,240 ± 35
AMS_5a	Tay 220	2.5-3.5	91-95	366.5	Poz-54258	5,440 ± 100	0.18	80% pollen	5,951-6,414	6,224 ± 118
AMS_34	**Tay 254**	**2.5-3.5**	**78-88**	**385.25**	**Poz-62560**	**6,000 ± 50**	**0.5**	**85% pollen**	**6,720-6,975**	**6,840 ± 66**
AMS_6	**Tay 220**	**3.5-4.5**	**0-9**	**412**	**Poz-55863**	**6,880 ± 40**	**0.4**	**80% pollen**	**7,620-7,818**	**7,712 ± 44**
AMS_7	**Tay 220**	**3.5-4.5**	**13-20**	**424**	**Poz-55864**	**7,080 ± 50**	**0.4**	**50% pollen**	**7,796-8,001**	**7,903 ± 49**
AMS_8a	**Tay 220**	**3.5-4.5**	**48-50**	**456.5**	**Poz-54259**	**7,100 ± 50**	**na**	**50% pollen**	**7,835-8,014**	**7,931 ± 49**
AMS_26	**Tay 254**	**3.5-4.5**	**24-34**	**459.5**	**Poz-62561**	**6,950 ± 50**	**0.8**	**70% pollen**	**7,680-7,925**	**7,780 ± 61**
AMS_40	*Tay 220*	*4-5*	*47-48*	*496*	*Poz62348*	*8,910 ± 70*	*0.3*	*mollusc*	*9,772-10,221*	*10,022 ± 122*
AMS_47a	*Tay 254*	*4-5*	*14.5-20.5*	*497.5*	*Poz-79041*	*9,110 ± 50*	*0.7*	*mollusc*	*10,408-10,195*	*10,263 ± 61*
AMS_47	**Tay 254**	**3.5-4.5**	**66.5-72**	**497.5**	**Poz-79427**	**7,450 ± 60**	**0.14**	**50% pollen**	**8,171-8,385**	**8,272 ± 62**
AMS_54	Tay 220	4.5-5.5	1-5	520.5	Poz-87385	6,670 ± 35	0.4	80% pollen	7,476-7,595	7,538 ± 31
AMS_50	Tay 254	4-5	38.5-45.5	521.25	Poz-79482	8,270 ± 50	na	50% pollen	9,091-9,430	9,265 ± 93
AMS_19	**Tay 220**	**4-5**	**87-90**	**537**	**Poz-55868**	**7,590 ± 40**	**na**	**50% pollen**	**8,341-8,453**	**8,395 ± 28**
AMS_14c	*Tay 220*	*5-6*	*0-4*	*559.5*	*Poz-55870*	*7,390 ± 60*	*0.2*	*60% charred plant particles*	*8,045-8,347*	*8,226 ± 80*
AMS_14p	**Tay 220**	**5-6**	**0-4**	**559.5**	**Poz-55869**	**7,660 ± 40**	**0.5**	**80% pollen**	**8,393-8,540**	**8,449 ± 42**
AMS_35	**Tay 254**	**4.5-5.5**	**44-54.5**	**566.5**	**Poz-62563**	**7,670 ± 70**	**0.4**	**80% pollen**	**8,375-8,591**	**8,470 ± 60**
AMS_16.1 NPP	*Tay 220*	*4.5-5.5*	*67-69*	*587*	*Poz-55871*	*8,440 ± 80*	*0.2*	*75% non-pollen palynomorphs*	*9,265-9,549*	*9,450 ± 82*
AMS_16.1 Ruppia	*Tay 220*	*4.5-5.5*	*67-69*	*587*	*Poz-55872*	*8,280 ± 50*	*0.7*	*6 Ruppia seeds*	*9,095-9,436*	*9,283 ± 92*
AMS_16.2	**Tay 220**	**4.5-5.5**	**67-69**	**587**	**Poz-55874**	**7,880 ± 70**	**0.2**	**80% pollen**	**8,549-8,981**	**8,716 ± 124**
AMS_36	**Tay 254**	**4.5-5.5**	**66-76**	**589.5**	**Poz-62564**	**7,940 ± 60**	**0.5**	**50% pollen**	**8,610-8,992**	**8,799 ± 110**
AMS_36c	*Tay 254*	*4.5-5.5*	*66-76*	*589.5*	*Poz-62566*	*8,330 ± 80*	*0.3*	*90% charred plant particles*	*9,500-9,092*	*9,333 ± 107*
AMS_17	*Tay 220*	*4.5-5.5*	*89-95*	*609*	*Poz-55875*	*7,410 ± 60*	*0.3*	*35% pollen, 35% tissues*	*8,050-8,374*	*8,247 ± 73*
S1-tephra*	**Tay 253**	**5-5.3**	**25-30**	**616**	**-/-**	**8,049 ± 49**	**na**	**terrestrial plant remains**	**8,725-9,090**	**8,939 ± 83**

* Modelled age of the S1-tephra as defined in the Dead Sea record[11].

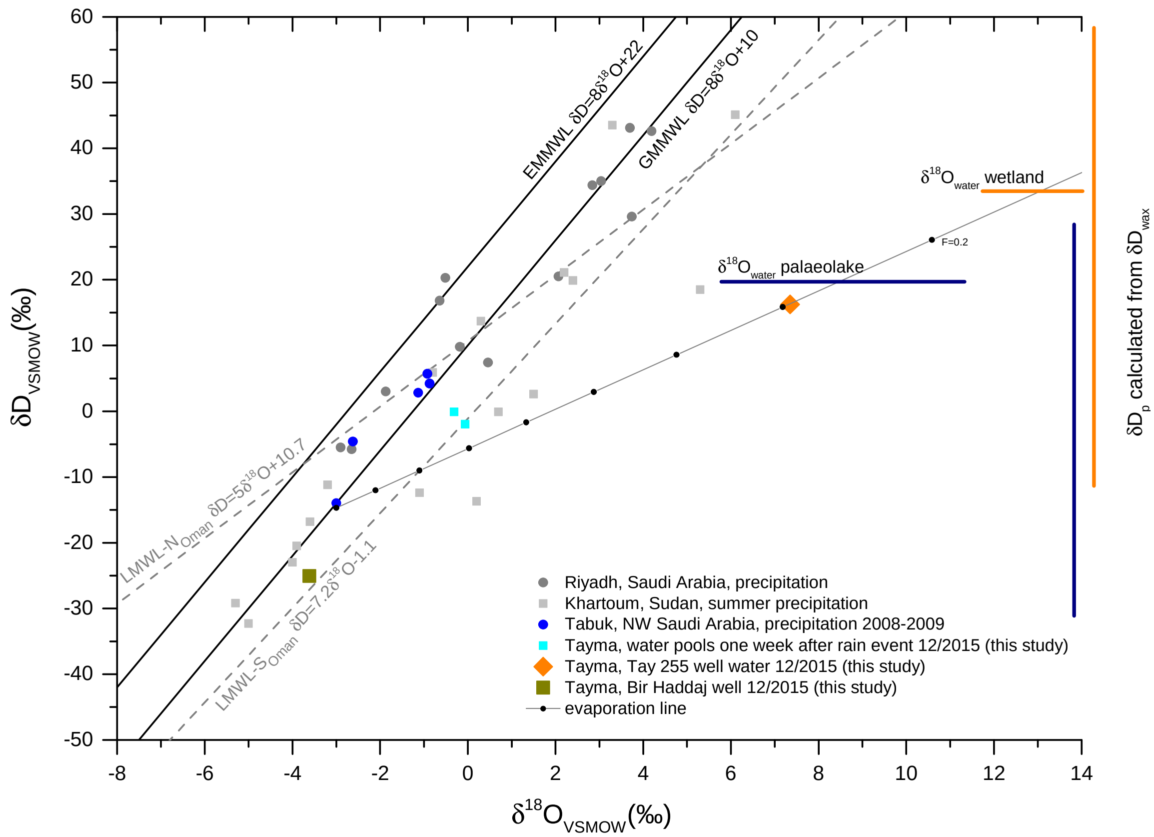

Supplementary Fig. 8: δD and $\delta^{18}O$ plot of Tayma palaeolake water and palaeo-moisture source reconstruction. For the isotopic characterisation of moisture sources, we used the Global Meteoric Water Line (GMWL) and Eastern Mediterranean Meteoric Water Line (EMMWL; high δD excess)[12], the two Local Meteoric Water Lines of rainstorm events in Oman[13], with LMWL-N (Mediterranean frontal systems; enriched δD) and LMWL-S (Indian Ocean cyclones and tropical depressions; depleted δD and $\delta^{18}O$), the Red Sea-influenced rainstorm events in Riyadh[14] (partly enriched δD), the composition of the African monsoon precipitation (data from Khartoum, Sudan; partly depleted δD)[15], and few available precipitation data from Tabuk, NW Saudi Arabia[15], very close to Tayma. Surface rainwater collected in water pools in a wadi SW of the Tayma palaeolake show $\delta^{18}O$ values of around -0.5‰ and slightly enriched δD values. The stable isotopes of the Bir Haddaj well in Tayma reflect sub-surface groundwater with -3.5‰ $\delta^{18}O$ and -24.6‰ δD, similar to the middle of the Saq aquifer[16,17]. Groundwater sampled at 1.5 m depth in the well of Tay 255 (in 2015) shows highly enriched values of +7.4‰ $\delta^{18}O_{water}$ (+16.2‰ δD), only slightly lower than the calculated mean $\delta^{18}O_{water}$ of +8.4‰ for the palaeolake surface water between 8,800 and 7,950 cal yr BP. In comparison, the modelled mean $\delta^{18}O_{water}$ of the wetland phase between 7,800 and 6,800 cal yr BP is extremely heavy (+13.1‰). The difference between both settings will be mainly influenced by changes in precipitation and evaporation. Past precipitation estimates (δD_p) based on δD_{wax} range between -28 and +44‰ for the deep lake phase and -11 and +58‰ for the wetland phase, which may indicate a change in the predominant atmospheric moisture source. We calculated an evaporation line between $\delta^{18}O_{water}$ = -3‰ for the groundwater-supported lake and +7.4‰ of Tay 255 well water and found a high evaporation rate of >70% for the surface water of the deep lake and >80% for the shallow lake phase that reflect highly arid conditions.

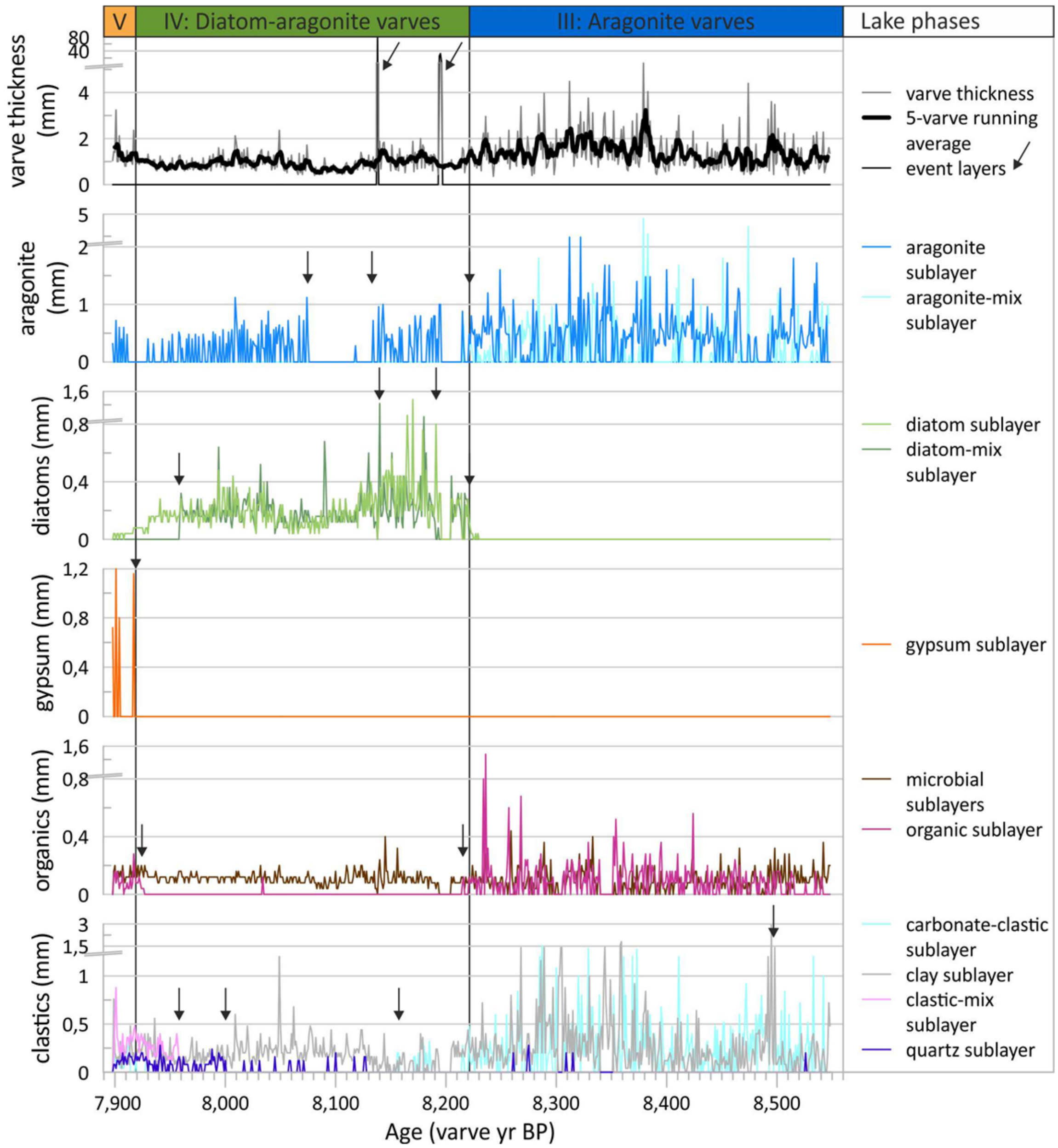

Supplementary Fig. 9: Varve micro-facies of lake phases III (aragonite varves), IV (diatom-aragonite varves) and V (transition to clastic-evaporitic lamination). Each varve (annual lamination) consists of at least two, but mostly three or more sublayers. Black arrows mark two several cm-thick graded event layers in the varve thickness panel (top); in the sublayer panels, arrows point either towards the onset or ceasing occurrence of a sublayer, or to particularly thick sublayers.

References

1. Engel, M. et al. The early Holocene humid period in NW Saudi Arabia – sediments, microfossils and palaeo-hydrological modelling. *Quat. Int.* **266**, 131–141 (2012).
2. Wellbrock, K. et al. in: *Taymāʾ I* (eds. Hausleiter, A., Eichmann, R. & al-Najem, M.) 145–198 (Archaeopress, 2018).
3. Al-Ahmadi, M. E. Hydrogeology of the Saq aquifer northwest of Tabuk, northern Saudi Arabia. *J. King Abdulaziz Univ. Earth Sci.* **20**, 51–66 (2009).
4. UN-ESCWA & BGR. *Inventory of shared water resources in Western Asia Ch 10* (Beirut, 2013).
5. Wellbrock, K., Strauss, M., Külls, C. & Grottker, M. in: *Des refuges aux oasis: Vivre en milieu aride de la Préhistoire à aujourd'hui. XXXVIIIe rencontres internationales d'archéologie et d'histoire d'Antibes* (eds. Purdue, L., Charbonnier, J. & Khalidi, L.) 231–249 (Éditions APDCA, 2018).
6. Vaslet, D. et al. *Geologic map of the Tayma quadrangle, sheet 27C: Kingdom of Saudi Arabia* (Ministry of Petroleum and Mineral Resources, 1994).
7. Engel, M. et al. Lakes or wetlands? A comment on 'The middle Holocene climatic records from Arabia: Reassessing lacustrine environments, shift of ITCZ in Arabian Sea, and impacts of the southwest Indian and African monsoons' by Enzel et al. *Global Planet. Change* **148**, 258–267 (2017).
8. Dinies, M., Neef, R., Plessen, B. & Kürschner, H. in *The Archaeology of North Arabia: Oases and Landscapes* (ed. Luciani, M.) 57–78 (Austrian Academy of Sciences Press, 2016).
9. Blaauw, M. & Christen, J. A. Flexible paleoclimate age-depth models using an autoregressive gamma process. *Bayesian Anal.* **6**, 457–474 (2011).
10. Reimer, P. J. et al. IntCal13 and Marine13 radiocarbon age calibration curves 0–50,000 Years cal BP. *Radiocarbon* **55**, 1869–1887 (2013).
11. Neugebauer, I. et al. Implications of S1 tephra findings in Dead Sea and Tayma palaeolake sediments for marine reservoir age estimation and palaeoclimate synchronisation. *Quat. Sci. Rev.* **170**, 269–275 (2017).
12. Gat, J. R. Oxygen and hydrogen isotopes in the hydrological cycle. *Annu. Rev. Earth Pl. Sc.* **24**, 225–262 (1996).
13. Weyhenmeyer, C. E., Burns, S. J., Waber, H. N., Macumber, P. G. & Matter, A. Isotope study of moisture sources, recharge areas, and groundwater flow paths within the eastern Batinah coastal plain, Sultanate of Oman. *Water Resour. Res.* **38**, 1184 (2002).
14. Michelsen, N. et al. Isotopic and chemical composition of precipitation in Riyadh, Saudi Arabia. *Chem. Geol.* **413**, 51–62 (2015).
15. IAEA & WMO. *Global Network of Isotopes in Precipitation. The GNIP Database.* https://nucleus.iaea.org/wiser (2018).
16. Alyamani, M. S. Isotopic composition of rainfall and ground-water recharge in the western province of Saudi Arabia. *J. Arid Environ.* **49**, 751–760 (2001).
17. Al-Sagaby, A. & Moallim, A. Isotopes based assessment of groundwater renewal and related anthropogenic effects in water scarce areas: Sand dunes study in Qasim area, Saudi Arabia. *IAEA-TECDOC* **1246**, 221–229 (2001).